Tribology International 62 (2013) 208–214

Contents lists available at SciVerse ScienceDirect

Tribology International

journal homepage: www.elsevier.com/locate/triboint

In situ thermal measurements of sliding contacts

Kyle G. Rowe, Alexander I. Bennett, Brandon A. Krick, W. Gregory Sawyer *

Department of Mechanical and Aerospace Engineering, University of Florida, Gainesville, FL 32611, United States

ARTICLE INFO

Article history:
Received 23 August 2012
Received in revised form
15 February 2013
Accepted 18 February 2013
Available online 5 March 2013

Keywords:
Temperature
Frictional heating
Infrared
Elastomer

ABSTRACT

This study examines frictional heating and the associated temperature rise for a sliding circular contact using an *in situ* thermal micro-tribometer. Observation of the contact temperature used a radiometric approach to measure local temperature at the sliding interface with an emphasis on full field imaging and thermal accuracy. Filled natural rubber samples were slid against optically smooth CaF_2 counter-samples. Temperature rise was measured for externally applied normal forces ranging from ~100 to 1000 mN and sliding velocities ranging from ~250 to 1000 mm/s, producing temperature rises between ~3 and 26 °C. Measured temperature rise was compared to the analytical models of Jaeger, Archard, and Tian and Kennedy for the average temperature rise in sliding contacts.

1. Introduction

Frictional heating and the temperature rise in a sliding contact is a fascinating, and often passionately debated, area of study. The effects of temperature on friction and wear are of significant practical interest; for example, moving mechanical assemblies and the materials selected for durable operation must survive not only the ambient conditions but also the thermal conditions generated as a result of frictional sliding. Numerous studies have shown that the real area of contact between two rubbing bodies is typically small compared to the apparent area of contact [1–7]. In these intimate contacts, friction and high contact pressures frequently combine to generate substantial flash temperatures, and these asperity contacts can have profound effects on the tribological operation [8]. Characterization of the dependence of tribological properties on such temperatures and pressures is an ongoing effort which has spanned analytical, numerical, and empirical approaches [9]. Here we expand these methods through precise micro-scale experiments by (1) directly measuring the temperature profile of the apparent contact area for small contacts, (2) correlating the measured temperature data with traditional tribotesting (*i.e.* friction/wear) measurements, and (3) comparing these measurements to the established models for frictional heating. These measurements not only provide explicit temperature and pressure profiles within the contact, but can also provide data for estimates of wear.

Solutions to heat transfer problems involving moving sources of heat have been of great importance in the understanding of frictional heating. The early work of Jaeger [10] used an approach based upon the superposition of various classical heat transfer source types to solve for the average temperature rise in the contact due to moving sources of various shapes and uniform distributions; his work was largely based upon the fundamentals proposed by Carslaw [11]. Postulates put forth by Blok [8,12,13] and Holm [14] expanded on the thermodynamic and geometric intricacies of the problem. Archard [15] used simple physical considerations in deriving practical equations for surface temperature rise with functional forms similar to those of Blok and Jaeger. Tian and Kennedy later expanded upon these models for the entire range of Peclet numbers using a Green's theorem approach [16]. More recently Bansal and Streator [17] used a numerical approach to evaluate the heat partitioning hypotheses used by Blok and Jaeger, in addition to determining the accuracy of Tian and Kennedy's approximate formula for the maximum interfacial temperature rise for various source shapes and distributions. One challenge associated with the use of contact temperature models is deciding how heat is partitioned within the contact. It was originally postulated by Blok that no temperature discontinuity should exist between two materials in areas of real contact, and that a constant overall heat partition function could be estimated by equating the maximum surface temperatures of the two bodies within the contact [13]. Although this method provides a good estimate, the most accurate partitioning of heat matches the temperature at every point within the real area of contact and does not require the use of a partition function [9,17–19].

The progression of empirical analysis for this problem has evolved alongside theoretical solutions. These experiments have spanned a large range of methods starting with embedded thermocouples, which then progressed to the use of dynamic

* Corresponding author. Tel.: +1 352 392 8488; fax: +1 352 392 1071.
E-mail address: wgsawyer@ufl.edu (W. Gregory Sawyer).

0301-679X/$ - see front matter © 2013 Elsevier Ltd. All rights reserved.
http://dx.doi.org/10.1016/j.triboint.2013.02.028

and thin-film thermocouples [20–22]. The radiometric approach, which is considered to be the most accurate because of its ability to sample at higher speeds and capture larger areas, has been used recently but often at high temperatures (400–500 °C) and large variability [23–29]. Major limitations associated with using a radiometric approach include an incomplete knowledge of emissivity and real contact area of the contacting bodies [24,29–31]. We have attempted to develop a small scale, high precision radiometric approach for full field, direct temperature measurement of the contact.

Here, we have designed and constructed a new instrument that combines microtribological probes and methods to perform sliding friction experiments while making high fidelity full field surface temperature measurements of the contact through infrared thermography. The instrument is capable of measuring normal and friction forces ranging from 10 μN to over 2 N. This design facilitates synchronized measurement of externally applied contact force, friction force, and *in situ* thermal imaging of the contact with a spatial resolution limited by the diffraction limit (around 3 μm). Preliminary tribological tests with *in situ* frictional heating measurements were performed between half spheres of filled natural rubber and a flat calcium fluoride disk to directly obtain the temperature distribution and average temperature rise within the contact and compare these to the models previously set forth.

2. Tribometer description

The *in situ* thermal micro-tribometer is capable of performing pin-on-disk and reciprocation sliding experiments with *in situ* thermal imaging (Fig. 1). The hemispherical sample (pin) is mounted directly to an instrumented cantilever that measures normal and frictional forces. Three micrometer stages control the positioning and loading of the sample. Opposing the sample is a rotary stage which holds a flat calcium fluoride counter-sample (disk). An infrared camera focuses through the infrared transparent counter-sample onto the interface created by the pin and the disk via a 3X objective.

2.1. Imaging methodology and temperature analysis

When the sample and counter-sample are in sliding contact, nearly all the work done to overcome friction causes temperature rises at or near the interface in areas of true contact [15]. Thermal radiation from the surface of the sample is transmitted through the IR transmissive counter-sample and is focused onto an infrared detector. Calcium fluoride was used as the counter-sample due to its hardness, thermal conductivity, and ability to transmit light over wavelengths measured by the thermal camera.

There are three main contributions to the radiant energy collected by the infrared detector: (1) radiation from the rubber sample (pin), (2) the calcium fluoride counter-sample, and (3) reflected ambient radiation. The contribution of the counter-sample was neglected due to its low emissivity, even at elevated temperatures (approximately zero at 373 K) [32]. Thermal images taken before the materials were in contact were averaged and subtracted from subsequent images taken during sliding; greatly reducing the effect of the reflected radiation component; secondary reflection effects were neglected all together. The measured radiation is then only a function of the sample temperature and emissivity. An in-depth discussion of infrared thermography is given by Volmer [33].

The emissivity of the pin was determined by two different techniques. The first method compared surface temperature measurements made by the camera to measurements made by a thermal couple. In the second method a body of known emissivity and sample material were simultaneously imaged using the infrared camera. The emissivity of the sample material was adjusted in the camera software until the surface temperatures of both bodies were equal. Calibrations were done over the temperature range measured in this study (~20–70 °C) and through a calcium fluoride window to account for thermal and absorption effects. The emissivity of the nascent surface was determined to be close to 1 (~0.97) with no discernible dependence on temperature over the range considered. There was no perceptible difference between the emissivity of the sample before and after sliding.

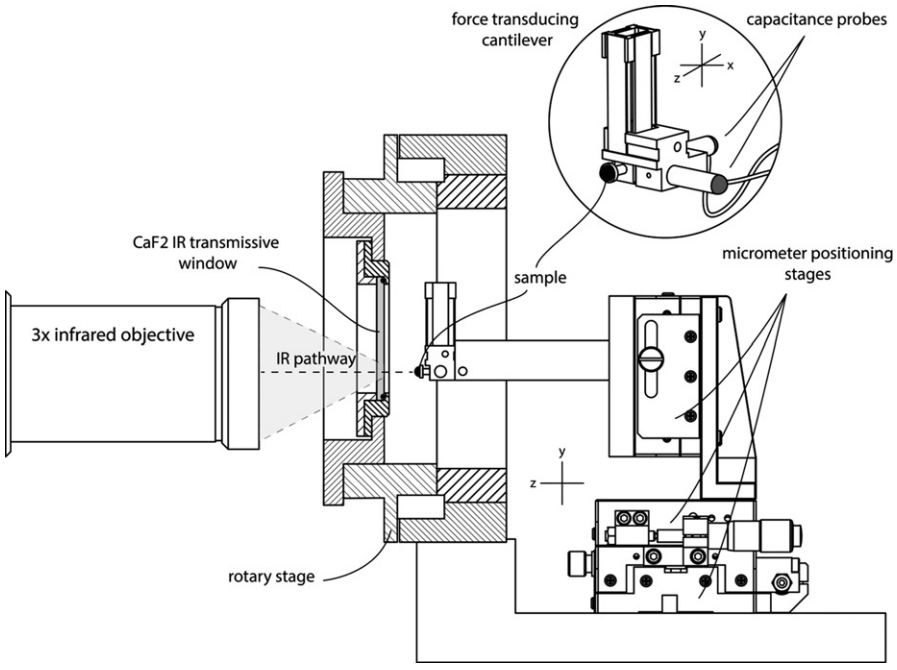

Fig. 1. Profile of tribometer (stage and counter-sample holder cross-sectioned). Radiation from sample/counter-sample sliding contact is focused onto the detector by the 3X camera lens.

Thermal images of the sliding contact were acquired by a FLIR SC7650 with an InSb detector as quickly as 100 Hz with a field of view of 3.2 mm × 2.4 mm and a 5 μm/px resolution. To approximate the nominal area of contact and the temperature distribution a post processing technique was performed. Plateau equalization, a general class of histogram-based mappings, was applied to gray scale temperature images to provide contrast enhancement [34] of the distinct thermal gradients that exist at the edges of contact. Edge detection was then used to estimate an outline of the nominal contact area. Each pixel encompassed by the resulting contact outline was then mapped to the corresponding value from the measured temperature field. These values were considered representative of the nominal contact area as it was not likely that all of the material within this region was actually in intimate contact with the counter-sample. An average of all temperature values over the nominal contact area was considered the nominal contact temperature at that point in time. Likewise, the nominal contact pressure for each frame was calculated by dividing the measured force by the nominal contact area. This process was repeated for each time synced image of the contact.

The nominal contact temperature rise was calculated by subtracting the background temperature, the average contact temperature before sliding, from contact temperature values averaged over a specified amount of time corresponding to thermal steady state.

2.2. Force measurements and positioning metrology

Measurement of normal and tangential (friction) forces is accomplished with a displacement-based cantilever load head assembly. The cantilever assembly consists of two sets of parallel flexures affixed (at 90° off-sets) in series to constrain the flexure to rectilinear displacements (Fig. 1, inset). This design isolates the normal and tangential displacements to the flexures sensitive in that direction; making the two force measurements independent and decreases alignment uncertainties [35]. The free end of this cantilever serves to (1) secure the sample and (2) provide a conductive target for two capacitance probes. The capacitance probes monitor the normal and tangential displacements of the cantilever; these displacements are used to measure externally applied normal and tangential forces. Through cantilever selection, normal loads of 2 N or more can be applied for high load cantilevers and less than 30 μN for low load cantilevers. The combination of cantilevers and capacitive probes used in this study can measure forces with uncertainties less than 15 mN (0.8% of full scale) and resolutions which exceed this by a factor of 10. The resolution of normal and tangential forces is only limited by the capacitance probe resolution (analog to digital conversion) and stiffness of the interchangeable cantilevers.

An open aperture rotary stage is connected by a belt to a servo motor and controlled by a Xenus digital drive with an integrated PI controller. The stage rotates the counter-sample from 1–1200 rpm ± 1 rpm. The radial run-out of the stage is <8 μm and an adjustable counter-sample holder reduces the total run-out to <3 μm. Compliance of the cantilever can accommodate small displacement changes (e.g. surface roughness, leveling errors, etc.) without significantly affecting the applied load. Direct angular position measurements are made by an optical read head and a ring encoder with 0.0008° resolution capable of accurate measurements up to 637 rpm.

LabVIEW™ was used for experimental control and data acquisition. A 16-bit analog to digital acquisition device externally conditioned all force and position measurements. Force and position data was acquired at 1000 Hz and time synced with thermal imaging.

3. Materials

Carbon black filled natural rubber hemispheres of 2 mm radius were used in this study. The rubber had an elastic modulus of approximately 6.5 MPa, a thermal conductivity of 0.24 W/mK, and a thermal diffusivity of 0.143×10^{-6} m^2/s. The average surface roughness and RMS roughness of the molded rubber were determined to be ~800 nm and ~1 μm, respectively, by scanning white light interferometer (Veeco Wyko NT9100).

Calcium fluoride was used as the infrared transparent counter-sample with 92–95% transmission of electromagnetic wavelengths in the range of 0.2–6.5 μm. The wavelengths of light measured in these experiments were in the range of 3–5 μm; this value was set by the infrared detector and associated filtering. The combination of transmission, hardness, and thermal conductivity of calcium fluoride made it a better choice for these experiments when compared to other IR transmitters such as zinc selenide, sodium chloride, silicon, and germanium. The optical windows were 50 mm in diameter and 3 mm thick with an RMS roughness of ~6.5 nm.

4. Description of loading and sliding experiments

Long time duration (900 s) testing was conducted to observe the effects of load and sliding velocity on the average nominal contact temperature rise. Due to the finite nature of the moving body (disk) it was expected that residual heat reentering contact would lead to higher temperatures than predicted by thermal models derived for an infinite half space. Short duration (~25 s) and forced convection tests were performed to evaluate this effect by minimizing this redundant heating.

Prior to sliding, the sample was loaded against a clean calcium fluoride disk to a prescribed force at a track radius of 18 mm; radial position was the same for each experiment. A record of the surface temperature at ambient was taken before sliding. Experiments were then performed at prescribed speeds and loads for either short durations (25 s) or long durations (900 s). Images were acquired before, during, and after sliding at a rate of 80 Hz for short tests and 0.5 Hz for long duration tests. Experiments were performed at targeted loads of 100, 250, 500, 750, and 1000 mN with varying sliding velocities of 250, 500, 750, and 1000 mm/s. Forced convection testing was performed under these same conditions for a target normal load of 500 mN and a sliding velocity of 750 mm/s. During sliding a steady flow of laboratory air (~20 °C) was directed onto the disk surface just outside of contact via a fan and nozzle configuration. The flow of air was not measured but it was sufficient enough to cool exiting disk material down to ambient temperature before it reentered the contact. This was verified by a small drop of black paint placed on the disk surface just outside of the contact path.

Acquired images were post processed using MATLAB® to determine the average temperature over the nominal area of contact, estimated contact area, and nominal contact pressure (applied load over measured nominal contact area). Although normal force was measured throughout the experiments it was not adjusted during sliding to minimize disturbances to the system.

5. Results

An overview of the measured contact temperature as a function of applied load and sliding velocity is shown in Fig. 2. Nominal contact temperature rises ranged from ~3 °C, at the lowest load and sliding velocity, to ~26 °C, coinciding with the

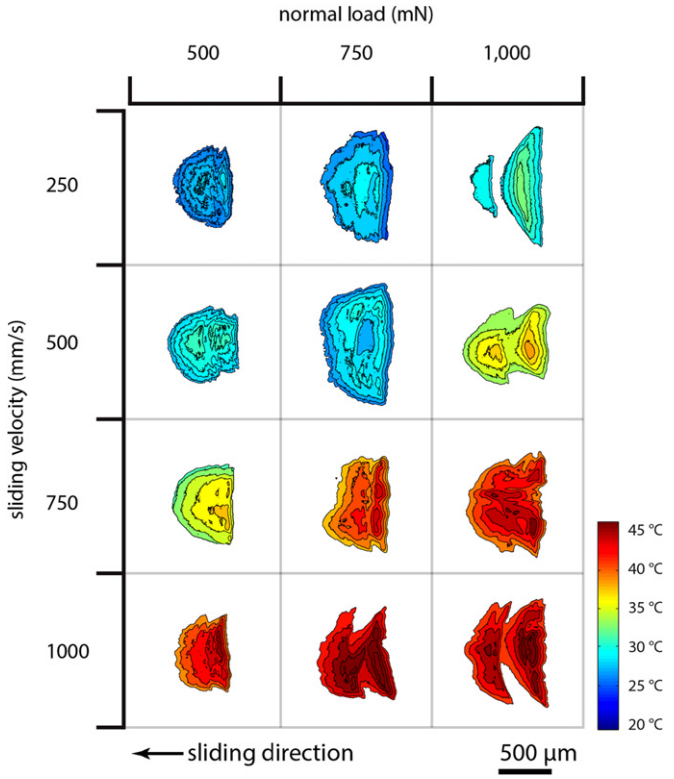

Fig. 2. Isotherms show the development of the nominal contact temperature and the nominal contact area for various applied loads and sliding velocities. Each image, representative of the test, was taken from a single frame near the end of sliding from selected long duration (900 s) experiments. With increasing velocity and normal load the contact distorted from its original elliptical shape to a band shape with a distinct leading edge. The average contact temperature rise ranged from 3 to ~26 °C with the friction coefficient, contact pressure, and sliding velocity having a prominent effect on the measured temperature increase.

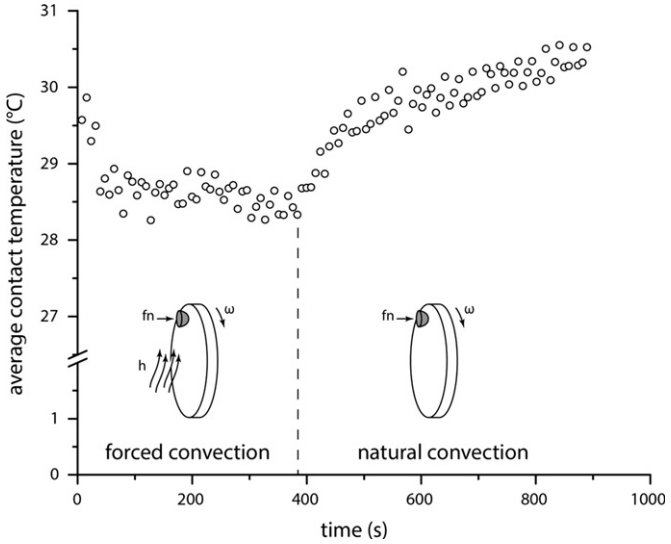

Fig. 3. Comparison of average contact temperature under forced and natural convection for a normal load of 500 mN and a sliding velocity of 750 mm/s. Friction coefficient, contact pressure, and sliding velocity did not significantly change over the duration of the experiment (σ=0.06, 0.02 MPa, and 0.5 mm/s respectively); providing a good estimate of the effect of heated material reentering the contact on the measured contact temperature.

greatest product of friction coefficient, contact pressure, and sliding velocity. The maximum single point temperature was measured to be ~51 °C. Short duration and forced convection tests resulted in a reduced contact temperature and time required to reach steady state (Fig. 3). Friction coefficient contact pressure, and sliding velocity did not significantly change over the duration of the convection experiment (σ=0.06, 0.02 MPa, and 0.5 mm/s respectively); providing a good estimate of the effect of heated material reentering the contact on the measured contact temperature. Average measured values for each pin-on-disk experiment are given in Table 1.

During these experiments the observed shape of contact was distorted from an elliptical shape at low loads and sliding velocities, into a bifurcated contact with a distinct leading edge at the highest loads and velocities. This distortion of the contact was confirmed by separate images taken of moving contacts, of the same material, with an optical interferometer [35]. At lower loads and velocities the degree to which this happened was less, resulting in the appearance of more material being in contact. At higher loads and velocities material just behind this leading ridge was at a sufficient distance from the counter-sample that it no longer appeared to be in contact. These contact shapes were most likely due to the accommodation of strain by the material as a result of low modulus and large interfacial shear stresses. Schallamach observed a similar behavior between butyl rubber sliding on Perspex [36].

Over the duration of testing no visible wear debris was generated. Scanning white light interferometer scans confirmed the surface roughness of the rubber pin did not change significantly from the beginning to the end of the experiments (RMS ~ 900–1100 nm).

6. Discussion

A significant obstacle facing full field frictional heating measurements is the real-time measurement of the true area of contact. Classical contact mechanics may be used to estimate the area of contact but for highly deformable or rough surfaces, where the true area of contact may be significantly increased or reduced, it is not easily determined [4,7,35,37]. The present experimental configuration allows for the direct measurement of contact temperature in addition to providing an estimate of the shape and area of contact. This creates a unique situation where all of the variables required for thermal modeling are either known *a priori* or measured *in situ*.

In this experimental configuration the disk is heated by a moving source and conduction from the pin. The pin is heated by a stationary source and cooled by oncoming cooler portions of the disk. Because the disk material is cool when it enters contact it must be quickly brought up to the temperature of the stationary surface. This results in the interfacial temperature rise being dominated by the removal of heat away from contact by the moving counter-sample.

Although most of the heat generated in the contact is conducted into the moving body, a fraction of the total heat flux goes into each body in contact. Blok hypothesized that the maximum surface temperatures of the two contacting bodies must be equal, and that an overall heat partitioning factor can be estimated [13]. Jaeger used a similar idea by equating the average temperature of contact of the two bodies to derive an overall heat partitioning factor [10]. Both postulates assume a fraction, α, of the heat flux generated (per unit time over the area of contact) passes into body 1 and the remaining fraction, $(1-\alpha)$, passes into body 2. The fraction alpha can be obtained by equating the interfacial contact temperature due to a moving heat source, with heat flux $q\alpha$ going into body 1, to the contact temperature due to a stationary heat source, with $q(1-\alpha)$ going into body 2. (Here the disk is taken as body 1 and the pin as body 2). Laraqi et al. [38] showed when the Peclet number was ≥ 30 that for any increase in velocity, and therefore Peclet number, the partitioning coefficient remains approximately constant.

Table 1
Average measured values from pin-on-disk experiments of a carbon black filled natural rubber half spheres on calcium fluoride. Listed values represent averages taken over the steady state portion of the experiment with calculated uncertainties, u, or standard deviations, σ.

Velocity [mm/s]	Fn [mN]	$\sigma(Fn)$ [mN]	μ	$\sigma(\mu)$	a [μm]	Nominal contact pressure [Mpa]	$u(P)$ [Mpa]	Pe	$u(Pe)$	Nominal contact temperature rise ΔT [°C]	$\sigma(T)$ [°C]
(a) Long duration sliding (~900 s)											
250	112	2	4.1	0.20	360	0.57	0.01	18	2	**3**	0.1
	211	2	3.2	0.05	320	0.88	0.01	20	1	**4**	0.1
	493	11	1.9	0.03	250	1.35	0.08	25	1	**5**	0.1
	755	13	1.9	0.10	250	1.34	0.10	31	1	**5**	0.1
	968	10	2.5	0.12	280	2.03	0.08	28	1	**8**	0.1
500	113	5	4.4	0.60	380	0.49	0.01	40	3	**5**	0.2
	493	11	2.1	0.10	260	1.26	0.07	51	1	**8**	0.1
	737	12	1.7	0.07	240	1.13	0.11	66	1	**9**	0.1
	1012	12	2.2	0.16	270	2.22	0.10	55	1	**13**	0.3
750	479	11	2.6	0.53	290	1.24	0.05	76	4	**12**	0.3
	758	11	2.7	0.48	290	1.64	0.06	84	1	**17**	0.2
	985	12	2.5	0.17	280	1.62	0.09	96	1	**18**	0.5
1000	509	12	2.8	0.23	300	1.44	0.05	98	5	**17**	0.5
	738	12	2.9	0.12	300	1.37	0.06	120	1	**19**	0.5
	846	7	2.3	0.06	270	1.30	0.07	132	1	**18**	0.4
	982	11	3.2	0.25	320	1.82	0.06	120	1	**26**	0.8
	996	7	2.5	0.07	280	1.87	0.08	120	1	**22**	0.7
(b) Short duration sliding (~25 s)											
500	474	3	2.3	0.20	440	0.78	0.01	64	4	**5**	0.1
	714	3	2.1	0.08	490	0.96	0.01	71	4	**6**	0.2
	978	3	2.0	0.06	510	1.19	0.01	74	4	**8**	0.1
750	539	3	2.6	0.10	410	1.01	0.01	90	5	**8**	0.2
	750	3	2.4	0.10	440	1.21	0.01	97	5	**10**	0.3
	991	3	2.2	0.05	500	1.30	0.01	107	6	**10**	0.2
1000	526	3	2.1	0.02	400	1.06	0.01	116	6	**9**	0.1
	775	3	1.9	0.04	420	1.40	0.02	121	7	**10**	0.3
	984	4	2.0	0.04	440	1.60	0.02	129	7	**12**	0.3

Frictional heating models developed by Jaeger, Archard, and Tian and Kennedy, used to predict the nominal contact temperature rise for various source shapes and distributions are plotted in normalized form with measured data in Fig. 4 (Appendix B). Values used in these calculations are listed in Table 1. The measured temperature rises from the short duration (~25 s) sliding experiments were very close to those predicted by modeling; however, long duration (~900 s) sliding experiments were observed to have higher temperature rises than model predictions. Differences between the experimental setup and model geometries involved in the derivation of these equations may account for this discrepancy. These models neglect convection of heat away from the interface, do not account for the residual heat in the disk that passes back through the contact with each revolution (infinite half space assumption), and are for model contact geometries (circular, square, etc.). Other models have been proposed that account for the finite nature of both bodies as the contribution to the contact temperature from residual heat can be quite significant [9,39,40]. Laraqi et al. developed an analytical solution for the temperature distribution in a pin-on-disk configuration and found that for $Pe \geq 20$ there is a distinct heat drag that develops in the disk. At sufficiently high speeds the temperature tends to its average value which corresponds to a thermal balance between the heat flux entering over the area of contact and the heat flux removed by convection [38]. The effect of convection on the average temperature of contact and the time required to reach equilibrium is shown in Fig. 3. It is shown that residual heat in the disk effectively re-heats the contact resulting in a higher than predicted equilibrium contact temperature. The use of forced convection allows disk material exiting the contact to cool back down to ambient temperatures before reentering; mimicking the effect of sliding on an infinite half space. In a like manner, short duration experiments are sufficiently long enough for the contact to reach a quasi-steady state value and short enough as to minimize the effects of residual heat in the disk.

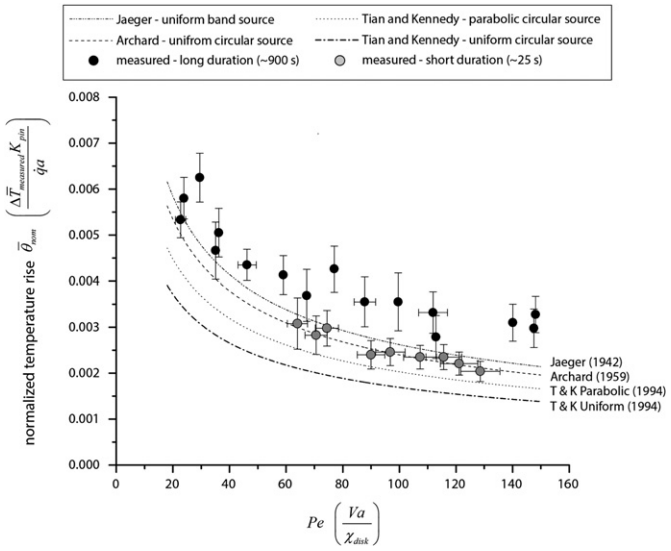

Fig. 4. Non-dimensional contact temperature rise comparison between direct measurements and model predictions. Long duration sliding leads to temperature rises greater than model predictions due to residual heat in the disk passing back through contact with each revolution. During short duration sliding events the disk temperature in the wake of contact does not have sufficient time to fully develop and as a result the average contact temperature values more closely follow modeled predictions.

It is not likely that the shape of contact and the pressure distribution is immaterial but to a good approximation the contact may be assumed as a uniform circular (or band shaped) source with a radius (half width), a, estimated from the measured nominal contact area, A, by approximating the entire contact as a circle ($a = \sqrt{A/\pi}$). It appeared that these assumptions had less of an influence on predicted temperature rise than other assumptions made above.

7. Concluding remarks

An *in situ* thermal micro-tribometer has been developed to accurately measure the full field temperature distribution between two contacting bodies due to frictional heating. Experiments were performed with filled natural rubber half spheres on smooth calcium fluoride to observe the effects of normal load, sliding velocity and friction coefficient on the average temperature rise of the interface.

A nominal contact temperature rise as high as 26 °C was observed with a maximum single point temperature of ~51 °C occurring at a point close to the leading edge of contact. The measured average contact temperature rise was compared to predicted values from Archard, Jaeger, and Tian and Kennedys' fundamental frictional heating models. *In situ* radiometric images taken of the sliding interface showed that models proposed by Jaeger and Archard for a uniform source moving over an infinite half plane provided the closest approximation of the nominal contact temperature rise for short duration sliding. Due to continuous reheating of the contact, long duration sliding experiments resulted in a higher than predicted nominal contact temperature rise.

Acknowledgments

The authors gratefully acknowledge Alex Webber and Jereme King at the University of Florida for their assistance in preliminary experiments and instrumentation. Additionally, the authors are indebted to Dr. Dylan Morris and Dr. Olivier Gerardin from Michelin, for the many useful discussions and help in sample preparation. This work was supported by Michelin North Americas.

Appendix A. Nomenclature

a	radius of contact or heat source (m)
$A(=\pi a^2)$	area of contact or heat source (m^2)
V	velocity of contact or heat source (m/s)
K	thermal conductivity (W/mK)
χ	thermal diffusivity (m^2/s)
$Pe=Va/\chi$	non-dimensional speed parameter (Peclet number)
$\dot{q}=Q/A$	heat rate per unit area (W/m^2)
$\Delta\overline{T}$	nominal contact temperature rise (°C)
$\overline{\theta}$	normalized nominal contact temperature rise
$K^*=K_{disk}/K_{pin}$	non-dimensional thermal conductivity

Appendix B. Contact temperature derivations

The equations used in computing the normalized nominal contact temperature rises (Fig. 4) were derived using various solutions of Jaeger, Archard, and Tian and Kennedy. These heat transfer solutions were used in conjunction with Jaeger's method of equating the nominal contact temperature of each body to estimate an overall heat partitioning coefficient α. A fraction of the heat generated in the contact, α, goes into the body experiencing the moving source and the remaining fraction, $(1-\alpha)$, goes into the body experiencing the stationary source. This constant heat partitioning coefficient was then used with moving source solutions to estimate the nominal contact temperature rise. Either the moving source or stationary source solution may be used in computing the temperature rise as the condition of matching the nominal temperatures of contact will guarantee that both solutions will be the same.

Measured temperature rise

The measured nominal contact temperature rise, Fig. 4, was normalized to the maximum temperature due to a stationary circular source of uniform distribution in the following way

$$\overline{\theta}_{nom}=\frac{\Delta\overline{T}_{measured}K_{pin}}{\dot{q}a}. \tag{B1}$$

Jaeger [10]

Jaeger's approximate band source solution, Eq. (B2), and Tian and Kennedys' stationary uniform circular source solution, Eq. (B3), were used to compute an overall heat partitioning coefficient α

$$\Delta\overline{T}_{nom}=\frac{1.064\dot{q}a}{K}Pe^{-1/2} \tag{B2}$$

$$\Delta\overline{T}_{nom}=\frac{8\dot{q}a}{3\pi K} \tag{B3}$$

An estimate of the heat partitioning coefficient α was determined by setting Eqs. (B2) and (B3) equal with a fraction of the heat, $\alpha\dot{q}$, going into the disk and the remaining fraction, $(1-\alpha)\dot{q}$, going to the pin:

$$\frac{1.064\dot{q}\alpha a}{K_{disk}}Pe^{-1/2}=\frac{8(1-\alpha)\dot{q}a}{3\pi K_{pin}} \tag{B4}$$

solving for α

$$\alpha=\frac{0.849K_{disk}\sqrt{Pe}}{0.849K_{disk}\sqrt{Pe}+1.064K_{pin}} \tag{B5}$$

using the coefficient from Eq. (B5) in the moving source solution, Eq. (B2), the estimated nominal contact temperature rise can be written as

$$\Delta\overline{T}_{nom}=\frac{0.903\dot{q}a}{0.849K_{disk}\sqrt{Pe}+1.064K_{pin}} \tag{B6}$$

A non-dimensional form of Eq. (B6) may be written by normalizing it to the maximum contact temperature rise due to a stationary circular source ($\dot{q}a/K_{pin}$) of uniform distribution

$$\overline{\theta}_{nom}=\frac{\Delta\overline{T}_{nom}K_{pin}}{\dot{q}a}=\frac{0.903}{0.849K^*\sqrt{Pe}+1.064}. \tag{B7}$$

Archard [15]

Equating Archard's solutions for the nominal contact temperature rise due to a stationary circular source of uniform strength, Eq. (B8), and the solution due to a fast moving circular source, Eq. (B9), it is possible to calculate an overall constant heat partitioning coefficient, α

$$\Delta\overline{T}_{nom}=\frac{Q_{pin}}{4aK_{pin}} \tag{B8}$$

$$\Delta\overline{T}_{nom}=\frac{0.31Q_{disk}}{K_{disk}a}Pe^{-1/2} \tag{B9}$$

equating the average nominal contact temperatures of Eqs. (B8) and (B9) and solving for α

$$\frac{0.31Q_{disk}\alpha}{K_{disk}a}Pe^{-1/2}=\frac{Q_{pin}(1-\alpha)}{4aK_{pin}} \tag{B10}$$

$$\alpha=\frac{0.785K_{disk}\sqrt{Pe}}{0.785K_{disk}\sqrt{Pe}+0.974K_{pin}} \tag{B11}$$

From this result the average contact temperature rise due to a uniform circular source, with the partitioning of heat being accounted for, is given by Eq. (B12). Normalizing this result to the maximum contact temperature rise due to a stationary circular source of uniform distribution Eq. (B13) is obtained

$$\Delta\overline{T}_{nom} = \frac{0.765\dot{q}a}{0.785K_{disk}\sqrt{Pe}+0.974K_{pin}} \tag{B12}$$

$$\overline{\theta}_{nom} = \frac{\Delta\overline{T}_{nom}K_{pin}}{\dot{q}a} = \frac{0.765}{0.785K^*\sqrt{Pe}+0.974}. \tag{B13}$$

Tian and Kennedy [16]

Tian and Kennedy derived equations for the nominal contact temperature rise over the entire range of Peclet numbers for circular heat sources of uniform (B14) and parabolic (B15) distributions [16]

$$\Delta\overline{T}_{nom} = \frac{1.22\dot{q}a}{K\sqrt{\pi(0.6575+Pe)}} \tag{B14}$$

$$\Delta\overline{T}_{nom} = \frac{1.464\dot{q}a}{K\sqrt{\pi(0.874+Pe)}} \tag{B15}$$

using Jaeger's method of partitioning for the case of the uniform circular source:

$$\frac{1.22\alpha\dot{q}a}{K_{disk}\sqrt{\pi(0.6575+Pe)}} = \frac{1.22(1-\alpha)\dot{q}a}{K_{pin}\sqrt{\pi(0.6575)}} \tag{B16}$$

$$\alpha = \frac{0.849K_{disk}\sqrt{Pe+0.6575}}{0.849K_{disk}\sqrt{Pe+0.6575}+0.688K_{pin}} \tag{B17}$$

an estimation of the nominal contact temperature rise due to a circular source with a uniform distribution, Eq. (B18), was obtained by substituting $\alpha\dot{q}$ for $\dot{q}$ and K_{disk} for K in Eq. (B14)

$$\Delta\overline{T}_{nom} = \frac{0.584\dot{q}a}{0.849K_{disk}\sqrt{Pe+0.6575}+0.688K_{pin}} \tag{B18}$$

Normalizing the above equation in the same way as Eq. (B13) it may be expressed in non-dimensional form as

$$\overline{\theta}_{nom} = \frac{\Delta\overline{T}_{nom}K_{pin}}{\dot{q}a} = \frac{0.584}{0.849\cdot K^*\sqrt{Pe+0.6575}+0.688} \tag{B19}$$

Using the above procedures for calculating the heat partitioning coefficient and the nominal contact temperature rise, similar expressions may be written for the circular heat source with a parabolic distribution, Eq. (B20), with a non-dimensional form given by Eq. (B21)

$$\Delta\overline{T}_{nom} = \frac{0.730\cdot\dot{q}a}{0.884\cdot K_{disk}\sqrt{Pe+0.874}+0.826\cdot K_{pin}} \tag{B20}$$

$$\overline{\theta}_{nom} = \frac{\Delta\overline{T}_{nom}K_{pin}}{\dot{q}a} = \frac{0.730}{0.884\cdot K^*\sqrt{Pe+0.874}+0.826}. \tag{B21}$$

References

[1] Dyson J, Hirst W. The true contact area between solids. Proceedings of the Physical Society of London Section B 1954;67:309–12.
[2] Holm R. Electric contacts handbook. Berlin: Springer-Verlag; 1958.
[3] Bowden FP, Tabor D. The friction and lubrication of solids. London: Oxford Univ. Press; 1950.
[4] Chromik RR, Baker CC, Voevodin AA, Wahl KJ. *In situ* tribometry of solid lubricant nanocomposite coatings. Wear 2007;262:1239–52.
[5] McCutchen CW. Optical systems for observing surface topography by frustrated total internal reflection and by interference. Review of Scientific Instruments 1964;35:1340–5.
[6] O'callaghan PW, Probert SD. Prediction and measurement of true areas of contact between solids. Wear 1987;120:29–49.
[7] Wahl KJ, Chromik RR, Lee GY. Quantitative *in situ* measurement of transfer film thickness by a Newton's rings method. Wear 2008;264:731–6.
[8] Blok H. The flash temperature concept. Wear 1963;6:483–94.
[9] Kennedy F. Frictional heating and contact temperatures. modern tribology handbook, two volume set. Boca Raton: CRC Press; 2001.
[10] Jaeger JC. Moving Sources of heat and the temperature of sliding contacts. Journal and Proceedings of the Royal Society of New South Wales 1942;76:203–24.
[11] Carslaw H. Mathematical theory of heat conduction. London: MacMillan; 1921.
[12] Blok H. The dissipation of frictional heat. Applied Scientific Research 1955;5:151–81.
[13] Blok H. Theoretical study of temperature rise at surfaces of actual contact under oiliness lubricating conditions. In: Proceedings of the general discussion on lubrication and lubricants, vol. 2; 1937. p. 222–235.
[14] Holm R. Calculation of the temperature development in a contact heated in the contact surface, and application to the problem of the temperature rise in a sliding contact. Journal of Applied Physics 1948;19:361–6.
[15] Archard JF. The temperature of rubbing surfaces. Wear 1959;2:438–55.
[16] Tian XF, Kennedy FE. Maximum and averate flash temperatures in sliding contacts. Journal of Tribology—Transactions of the ASME 1994;116:167–74.
[17] Bansal DG, Streator JL. On estimations of maximum and average interfacial temperature rise in sliding elliptical contacts. Wear 2012;278–279:18–27.
[18] Bos J, Moes H. Frictional heating of tribological contacts. Journal of Tribology 1995;117:171–7.
[19] Ling F. A quasi-iterative method for computing interface temperature distributions. Journal of Applied Mathematics and Physics (ZAMP) 1959;10:461–74.
[20] Guha D, Roy Chowdhuri SK. The effect of surface roughness on the temperature at the contact between sliding bodies. Wear 1996;197:63–73.
[21] Schreck E, Fontana RE, Singh GP. Thin-film thermocouple sensors for measurement of contact temperature during slider asperity interaction on magnetic recording disks. IEEE Transactions on Magnetics 1992;28:2548–50.
[22] Tong HM, Arjavalingam G, Haynes RD, Hyer GN, Ritsko JJ. High-temperature thin-film Pt–Ir thermocouple with fast time response. Review of Scientific Instruments 1987;58:875–7.
[23] Siroux M, Kasem H, Thevenet J, Desmet B, Dufrenoy P. Local temperatures evaluation on the pin–disc interface using infrared metrology. International Journal of Thermal Sciences 2011;50:486–92.
[24] Nagaraj HS, Sanborn DM, Winer WO. Direct surface temperature measurement by infrared radiation in elastohydrodynamic contacts and the correlation with the blok flash temperature theory. Wear 1978;49:43–59.
[25] Quinn TFJ, Winer WO. An experimental study of the hot spots ocurring during the oxidational wear of tool steel on sapphire. Journal of Tribology—Transactions of the ASME 1987;109:315–20.
[26] Floquet A, Play D. Contact temperature in dry bearings—3 Dimensional theory and verification. Journal of Lubrication Technology—Transactions of the ASME 1981;103:243–52.
[27] Gulino R, Bair S, Winer WO, Bhushan B. Temperature measurement of microscopic areas within a simulated head tape interface using infrared radiometric technique. Journal of Tribology—Transactions of the ASME 1986;108:29–34.
[28] Ingram M, Reddyhoff T, Spikes HA. Thermal behaviour of a slipping wet clutch contact. Tribology Letters 2011;41:23–32.
[29] Reddyhoff T, Spikes HA, Olver AV. Compression heating and cooling in elastohydrodynamic contacts. Tribology Letters 2009;36:69–80.
[30] Bair S, Green I, Bhushan B. Measurement of asperity temperatures of a read write head slider bearing in hard magnetic recording disks. Journal of Tribology—Transactions of the ASME 1991;113:547–54.
[31] Bhushan B. Introduction to tribology. New York: John Wiley & Sons; 2002.
[32] Pukhonin VV, Chaikin AS. Spectral emissivity of LiF, CaF2, and NaCl crystals and fused quartz in the range 2–25 μ. Journal of Applied Spectroscopy 1972;16:106–9.
[33] Vollmer M, Möllmann K-P. Infrared thermal imaging. Weinheim: Wiley-VCH Verlag GmbH & Co. KGaA; 2010.
[34] Vickers VE. Plateau equalization algorithm for real-time display of high-quality infrared imagery. Optical Engineering 1996;35:1921–6.
[35] Krick BA, Vail JR, Persson BNJ, Sawyer WG. Optical *In Situ* micro tribometer for analysis of real contact area for contact mechanics, adhesion, and sliding experiments. Tribology Letters 2012;45:185–94.
[36] Schallamach A. How does rubber slide? Wear 1970:301–13.
[37] Wahl KJ, Sawyer WG. Observing interfacial sliding processes in solid–solid contacts (vol. 33, p. 1159, 2008). MRS Bullettin 2009;34:1159–67.
[38] Laraqi N, Alilat N, de Maria JMG, Baïri A. Temperature and division of heat in a pin-on-disc frictional device—exact analytical solution. Wear 2009;266:765–70.
[39] Ashby MF, Abulawi J, Kong HS. Temperature maps for frictional heating in dry sliding. Tribology Transactions 1991;34:577–87.
[40] Tian X, Kennedy F. Contact surface temperature models for finite bodies in dry and boundary lubricated sliding. Journal of Tribology 1993;115:411–8.